

## Highlights

### Noise Reduction in Wind Turbine Airfoils with Serrated Trailing Edges: An Experimental Study in Low Turbulence Wind Tunnel

Weicheng Xue, Hongyu Wang, Zhe Chen, Bing Yang<sup>\*1</sup>

- This study demonstrates that serrated trailing edges reduce noise effectively across a wider frequency range than previously reported, with significant reductions specifically confined by  $St_u = 1$  and  $St_l = 0.48$ .
- The effectiveness of serrated trailing edges in reducing noise varies with the angle of attack and airfoil profile, resulting in distinct noise reduction patterns in both frequency range and amplitude.
- The geometry of the serrations was found to have a negligible effect on noise reduction.
- Measurements reveal a clear correlation between reduced wake turbulence and noise reduction, indicating that serrated edges disrupt larger vortex structures responsible for generating noise.

---

<sup>1</sup>\*Bing Yang, corresponding author, bingyang1215@126.com

# Noise Reduction in Wind Turbine Airfoils with Serrated Trailing Edges: An Experimental Study in Low Turbulence Wind Tunnel

Weicheng Xue<sup>a,d</sup>, Hongyu Wang<sup>b</sup>, Zhe Chen<sup>d</sup>, Bing Yang<sup>\*1c,d</sup>

<sup>a</sup>*Pengcheng Laboratory, Shenzhen, Guangdong, 518055, China*

<sup>b</sup>*Internet Based Engineering, Beijing, 100083, China*

<sup>c</sup>*Goldwind Sci & Tech Co.,Ltd., Beijing, 101102, China*

<sup>d</sup>*Institute of Engineering Thermophysics, Chinese Academy of Sciences, Beijing, 100083, China*

---

## Abstract

This study explores the noise reduction achieved by airfoils with serrated trailing edges in a low turbulence wind tunnel, focusing on acoustic spectral characteristics and wake flow field measurements. We analyze the effects of various factors, including Reynolds number, angle of attack, serration parameters, and model type, on sound power levels and far-field radiation patterns. Our findings reveal that serrated trailing edges significantly reduce noise across a broader frequency range than previously documented, particularly in the mid-to-high frequency range, with reductions bounded by Strouhal numbers  $St_u = 1$  and  $St_l = 0.48$ . Interestingly, the serration geometry exhibits minimal impact on noise reduction, which varies with the angle of attack and airfoil profile across all tested conditions. Additionally, while serrations effectively lower noise levels, especially at higher frequencies, they do not significantly alter the airfoil's acoustic directivity patterns. Measurements of wake flow velocity spectra demonstrate a clear correlation between reduced wake turbulence and noise reduction, as serrated edges decrease the power spectral density of turbulent velocity fluctuations, effectively disrupting larger vortex structures responsible for noise generation. These valuable insights contribute to understanding the aerodynamic and acoustic benefits of serrated trailing edges, warranting further experimental validation in future studies.

---

<sup>1</sup>\*Bing Yang, corresponding author, bingyang1215@126.com

*Keywords:* wind turbine airfoil, serrations, noise reduction, aerodynamic noise, sound pressure level

---

## 1. Introduction

In the pursuit of enhancing wind turbine efficiency and productivity, there has been a noticeable trend towards increasing the size of wind turbines and extending blade lengths [1, 2]. As a result, the tip speed ratio of wind turbine rotors has been steadily rising [3]. However, aerodynamic noise generated by wind turbine blades increases with the fifth power of wind speed [4]. While higher tip speeds can improve wind turbine performance, they also lead to increased noise emissions. For instance, a 15% increase in the tip speed of wind turbine blades can result in a 3 dB rise in noise, which may adversely affect the living conditions of nearby residents [5].

The primary sources of noise in wind turbines are aerodynamic noise from the blades and mechanical noise from the nacelle [6]. Mechanical noise, stemming from the operation of mechanical components, is characterized by tonal qualities [7]. Conversely, aerodynamic noise arises from the interaction between air and the wind turbine blade and can be categorized into inflow turbulence noise and self-noise [8]. Within self-noise, turbulent and laminar boundary layer trailing edge noise are significant due to their origin from boundary layer interaction with the sharp trailing edge [9]. Stall separation noise and blunt trailing edge vortex shedding noise are less influential because wind turbines usually operate below stall conditions, and sharp trailing edges can mitigate vortex shedding noise.

Effective reduction of trailing edge noise is essential for optimizing wind turbine blade design. Several trailing edge modifications have been proposed to reduce noise while maintaining aerodynamic performance. These include brush trailing edges [10, 11, 12, 13], perforated trailing edges [13, 14, 15], and serrated trailing edges [16, 17, 18, 19, 20, 21]. Among these, serrated trailing edges have become particularly prominent due to their ability to effectively disrupt vortex formation and reduce noise levels, as well as their adaptable design options.

The efficacy of serrated trailing edges in mitigating aerodynamic noise has been investigated [22, 23, 16]. Gruber et al.[22, 23] reported noise reductions of up to 5 dB across a broad frequency spectrum, while Oerlemans et al.[16] conducted experiments on a full-scale 2.3 MW wind turbine, observing reductions of up to 3.2 dB below 1000 Hz. These studies demonstrate

that serrated trailing edges effectively reduce wind turbine noise, particularly at low to mid frequencies. However, their effectiveness diminishes at higher frequencies, where they can occasionally increase noise above critical levels, underscoring the need for further investigation.

Celik et al. [20] conducted experiments on a flat plate with a serrated trailing edge, finding that larger serrations significantly reduce noise. They noted that low-frequency analysis may need high-fidelity simulations for accuracy. However, discrepancies between current numerical and experimental results highlight the need for further investigation and a deeper understanding of the underlying noise reduction mechanisms.

Zhou et al. [24] investigated flexible trailing edge serrations on airfoils, finding that they achieve greater high-frequency noise reduction compared to rigid serrations. Additionally, they observed that flexible serrations align better with the flow, reducing crossflow intensity near the serration roots. However, selecting the appropriate flexibility depends on specific working conditions to ensure good stability of the serrations.

The geometry of serrated trailing edges plays a critical role in their noise reduction capabilities. Dassen et al.[25] found that serrated trailing edges on flat plates were more effective at noise reduction than those on airfoils. Finez et al.[26] explored various geometric parameters of serrated trailing edges on a cascade of seven NACA 651210 airfoils, discovering no significant impact of the cascade effect on noise reduction in the low to mid-frequency range. Singh et al.[27] examined non-uniform sinusoidal serrations, revealing that increased spanwise decoherence and vortex pairing resulted in greater noise reduction compared to uniform serrations. Gruber et al.[23] proposed design guidelines, emphasizing key parameters that influence noise reduction efficiency.

Significant advancements have been achieved in reducing tonal noise using serrated and porous trailing edges. Chong et al.[28] investigated the effects of serrated trailing edges on unsteady pure tone noise, particularly focusing on Tollmien-Schlichting waves and separation bubbles on a NACA 0012 airfoil at moderate Reynolds numbers ( $10^5 < Re_c < 10^6$ ). They found that serrations reduced instability noise by modifying the length scales of separation bubbles and suppressing their amplification. Additionally, the three-dimensional flow induced by serrations weakened normal fluctuations and adverse pressure gradients, further contributing to noise reduction. Subsequent studies[29, 30] demonstrated that non-planar serrated trailing edges accelerated the laminar-to-turbulent transition, further reducing noise levels. The trailing edge noise

followed a power law of velocity, underscoring its primary role as a noise source. Zhang and Chong [15] also examined the impact of porous parameters on tonal noise, identifying optimal settings for broadband noise reduction.

Despite significant advancements, the fundamental mechanisms behind noise reduction through modified trailing edges remain unclear. This study aims to enhance understanding by investigating the noise reduction mechanisms of wind turbine blade airfoils with serrated trailing edges. Experiments were conducted in an anechoic low turbulence wind tunnel using various airfoil models, including two wind turbine blade airfoils. The findings from this study will aid in optimizing trailing edge designs for noise reduction and developing low-noise wind turbine blades.

## **2. Experimental Apparatus and Procedure**

### *2.1. Anechoic wind tunnel*

The experiments were conducted in a small open-circuit anechoic low turbulence wind tunnel located at the Fluid and Acoustic Engineering Laboratory, Beihang University, as depicted in Fig. 1. The anechoic chamber has internal dimensions of  $8.9, \text{ m} \times 6.8, \text{ m} \times 4.65, \text{ m}$ , with a cutoff frequency of 200 Hz, ensuring minimal acoustic reflections during measurements. The wind tunnel, which extends from outside the chamber into its interior, features a circular outlet with a diameter of 150 mm and can achieve a maximum wind speed of 50 m/s. Table 1 provides the turbulence characteristics measured using a hot-wire anemometer at the center of the outlet, indicating a low turbulence intensity, which is critical for ensuring accurate flow and noise measurements. The experiments were carried out at wind speeds of 15 m/s, 25 m/s, and 35 m/s, with both noise and flow field measurements performed at each speed.

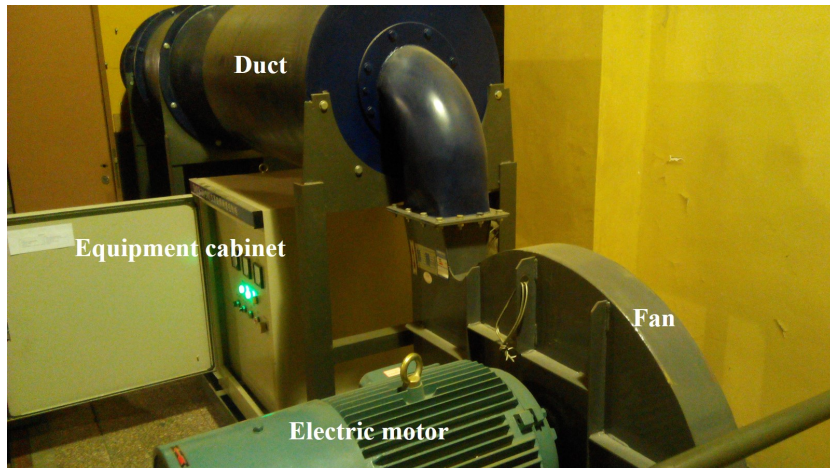


Figure 1: Wind tunnel and supporting measurement equipment

Table 1: Measured wind velocity and corresponding turbulence intensity at the wind tunnel outlet

Wind Velocity, m/s	15.19	25.12	35.45	45.69
Turbulence intensity, %	0.036	0.080	0.101	0.144

In Table 1, the measured turbulence intensity values demonstrate that the undisturbed flow remains well-controlled, even at higher wind speeds, with minimal turbulence interference. These low inflow turbulence levels are crucial to the experimental design, as the study specifically focuses on noise reduction in low inflow turbulence conditions.

Fig. 2 compares the sound pressure level of the sound pressure signal, denoted as  $L_p$ , in the anechoic chamber with and without a NACA 634421 airfoil at wind speeds of 25.12 m/s and 35.45 m/s. The sound pressure level  $L_p(f)$  at a frequency  $f$  is derived from the sound pressure signal captured by a microphone and is calculated using the formula shown in Eq. 1:

$$L_p(f) = 20 \log_{10} \left( \frac{|P(f)|}{p_0} \right) \quad (1)$$

where  $P(f)$  is the frequency domain representation of the sound pressure signal, obtained by applying the Fast Fourier Transform (FFT) to the time-domain signal  $p(t)$ , measured by the microphone. Specifically,  $P(f) = \text{FFT}(p(t))$ , and the magnitude  $|P(f)|$  represents the amplitude of the sound

pressure at frequency  $f$ . The reference sound pressure  $p_0$  is typically set to  $20 \mu\text{Pa}$ . The sound pressure level  $L_p(f)$ , expressed in decibels (dB), is then calculated by comparing  $|P(f)|$  to  $p_0$ , using a logarithmic scale to reflect the human auditory system’s sensitivity to sound.

The data acquisition and calculation of  $L_p(f)$  in this formula were efficiently performed using a custom LabVIEW program, which can be found at <https://doi.org/10.5281/zenodo.13768804>. Interested readers can refer to this program for more details.

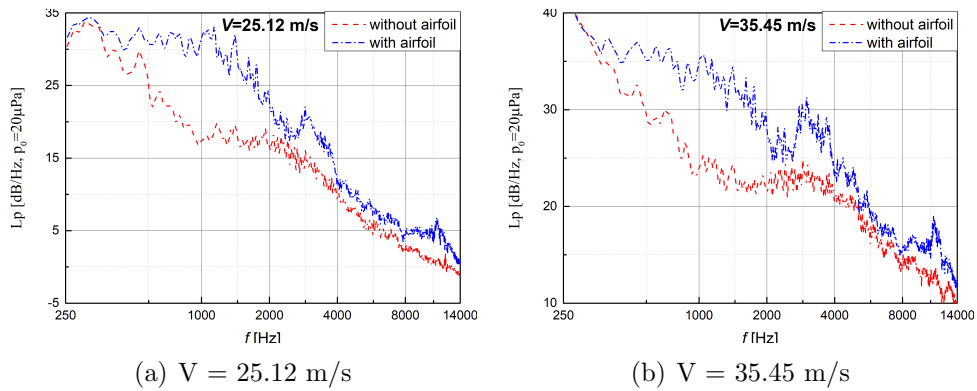


Figure 2: Spectral comparison of background and airfoil noise

Below 400 Hz, the presence of the airfoil has a negligible effect on noise levels. However, within the 400 to 4000 Hz range, the airfoil induces a significant noise increase, exceeding 10 dB at both tested wind speeds. In the 4000 to 8000 Hz range, the noise rise is more moderate, between 1 and 3 dB, while from 8000 to 14,000 Hz, the increase is approximately 5 to 6 dB. These findings indicate that the airfoil’s influence on noise is more pronounced at mid to high frequencies, and the overall noise level increases with wind speed. The maximum difference observed was 13.8 dB at the higher wind speed. The airfoil-generated noise exhibited a unique pattern, characterized by multiple narrowband tonal components superimposed on a broadband noise spectrum. It is crucial to ensure that serrated trailing edges are effective in reducing both broadband noise and narrowband tonal components, and to further investigate the mechanisms behind this noise mitigation.

## 2.2. Experimental Airfoils

The experimental setup featured two wind turbine airfoil models, NACA 633418 and NACA 634421, each with a uniform chord length of 74 mm and a span of 160 mm. These models were precisely assembled from two halves, with flat plates welded to the top and bottom of the wind tunnel outlet to secure the airfoils in place. The trailing edges, designed with a blunt profile and a thickness of 1 mm, included a 0.6 mm slot to allow for the attachment of serrations of various sizes. This design enabled a detailed investigation into noise reduction techniques using different serrated trailing edges.

## 2.3. Serrated Trailing Edges

Various serration half-heights ( $h$ ) and wavelength-to-half-height ratios ( $\lambda/h$ ) were tested, with all serrated trailing edges uniformly designed to have a thickness of 0.6 mm for easy attachment to the airfoil. The models labeled with "S" correspond to serrated trailing edges, while those labeled with "F" represent straight bars at half the serration height. The model labeled "0-0" is the baseline configuration, which features the original airfoil without any modifications to the trailing edge. Detailed parameters are listed in Table 2.

Table 2: Serration and Straight Bar Parameters

Half-height, $h$ (mm)	Wavelength, $\lambda$ (mm)	$\lambda/h$	Model
4	3.2	0.8	4-1S
	1.6	0.4	4-2S
	-	-	4-0F
5	4.0	0.8	5-1S
	2.0	0.4	5-2S
	1.0	0.2	5-3S
	-	-	5-0F
6	4.8	0.8	6-1S
	2.4	0.4	6-2S
	1.2	0.2	6-3S
	-	-	6-0F
0	0	0	0-0

#### 2.4. Data acquisition and processing system

The noise measurement setup utilized BSWA MPA 416 pressure transducer microphones (1/4-inch radius, 20 to 20,000 Hz frequency range). Data acquisition was performed with a National Instruments (NI) system, comprising a PXIe-1071 chassis, a PXIe-8102 controller, and multiple PXIe-4496 data acquisition cards. Each PXIe-4496 card supported synchronous sampling across 16 channels with a rate of 204.8 kS/s, ensuring compliance with the frequency requirements for accurate noise measurement. The microphones and data acquisition instrument is shown in Fig. 3.



Figure 3: Data acquisition instrument and microphones

The sound signals from the microphones were processed and stored in *.tdms* format using a LabVIEW-based data acquisition program. For analysis, these *.tdms* files were imported into a LabVIEW-based FFT (Fast Fourier Transform) analysis tool, which allowed for parameter customization such as the starting point of the time segment, number of segments, sliding window, and reference channels. The data acquisition sampling rate was set at 65536 samples/s, with a time segment length of 4096 samples and a 10-second recording duration per data acquisition session. A spectral overlap rate of 50% was used to ensure smooth spectrum calculation and

effective averaging. The FFT analysis interface is shown in Fig. 4. The LabVIEW program used for data acquisition and FFT analysis is available at <https://doi.org/10.5281/zenodo.13768804>.

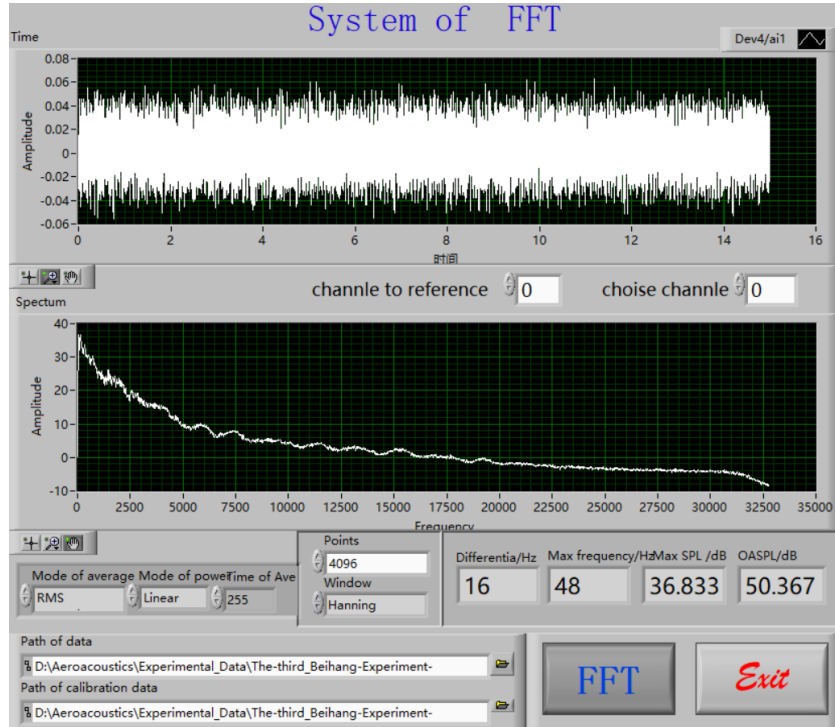


Figure 4: FFT analysis program interface

Noise analysis is usually conducted within specific frequency bands, either as doubling frequency bands with a 2:1 ratio between cutoff frequencies or as 1/3-octave bands, which divide these bands into three equal parts. This study adopts the 1/3-octave band approach. For a band centered at frequency  $f$ , the upper and lower cutoff frequencies are  $\sqrt[3]{2}f$  and  $f/\sqrt[3]{2}$ , respectively. This method enhances noise data precision. A high-pass filter with a cutoff frequency of 100 Hz is used, and the analysis spans 17 frequency bands, starting with a center frequency of 315 Hz.

The 1/3-octave band sound pressure level,  $L_p$ , is computed by summing the sound pressure levels within each frequency band. The energy summation in decibels (dB) for each 1/3-octave band is performed using Eq. 2:

$$L_p = 10 \log_{10} \left( \sum_{f_l \leq f_i \leq f_u} 10^{L_p(f_i)/10} \right) \quad (2)$$

In Eq. 2,  $L_p(f_i)$  represents the sound pressure level at frequency  $f_i$ , and the summation is performed over all frequencies within the lower and upper cutoff frequencies,  $f_l$  and  $f_u$ , of the 1/3-octave band. The exponential term converts the sound pressure level from decibels back to a linear scale, and the logarithmic operation returns the summed energy back into decibels. This method provides an accurate representation of the total energy within the 1/3-octave band.

The microphone arrangement in the experiment is shown in Fig. 5. The angle between the line connecting the microphones and the blade airfoil trailing edge, and the direction of the airflow, is denoted as  $\phi$ . Due to spatial constraints and equipment limitations within the wind tunnel, three microphones are positioned at a radius of 2.35 m from the model's trailing edge, corresponding to  $\phi$  angles of  $45^\circ$ ,  $60^\circ$ , and  $75^\circ$ , respectively. The placement of the microphones was further influenced by the insufficient distance between the wind tunnel outlet and the wall, making it impractical to position a microphone at the  $90^\circ$  angle due to its proximity to the wall. Consequently, in this experiment, when directivity is not a primary concern, the microphone located at the  $75^\circ$  position is used for acoustic data acquisition and subsequent processing. No corrections have been made to the sound pressure level equations.

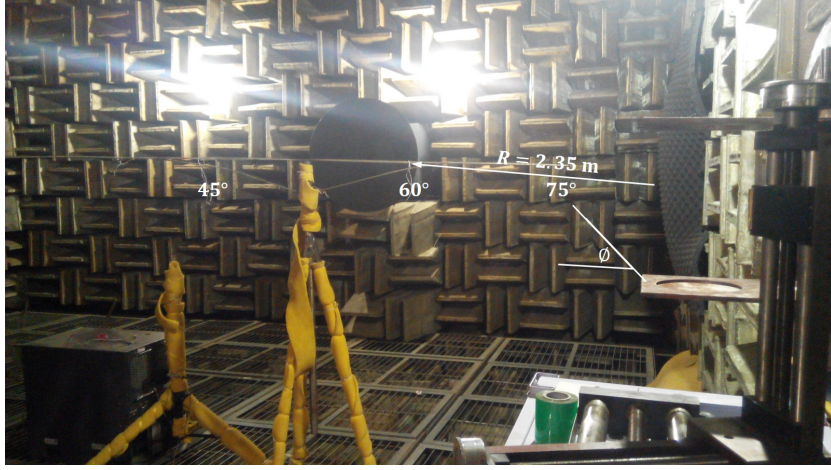


Figure 5: Microphone placement for directivity measurement

### 3. Noise Measurement

#### 3.1. Impact of Reynolds Number

The sound power levels for the NACA 633418 and NACA 634421 airfoils were measured at Reynolds numbers of  $0.7 \times 10^5$ ,  $1.2 \times 10^5$ , and  $1.6 \times 10^5$ . Fig. 6 and Fig. 7 show the 1/3-octave band sound power levels for the NACA 633418 and NACA 634421 airfoils, including configurations with trailing edge serrations, original airfoils, and those with added bars. Significant variations in the noise reduction performance of serrated trailing edges under different wind speed conditions can be observed. To better understand noise reduction across different frequencies and flow velocities, the noise frequency  $f$  was converted into the Strouhal number  $S_t$ , defined as:

$$S_t = \frac{f\delta}{U} \quad (3)$$

where  $f$  denotes the sound frequency,  $\delta$  represents the thickness of the boundary layer (assumed to be 3 mm in this study), and  $U$  is the inflow wind speed.

At lower Reynolds numbers, the NACA 633418 and NACA 634421 airfoils show primary noise reductions of 2~7 dB in the 630~1600 Hz range ( $0.12 \leq S_t \leq 0.32$ ). At moderate Reynolds numbers, the serrated trailing edge reduces noise by 2~5 dB in the 800~3150 Hz ( $0.096 \leq S_t \leq 0.38$ ) and 10000~12500 Hz ( $1.2 \leq S_t \leq 1.49$ ) ranges for both airfoil models. At higher Reynolds numbers, the serrated trailing edge is especially effective

in reducing tonal noise around 3150 Hz ( $St_t = 0.27$ ). Across all Reynolds numbers, airfoils with serrated trailing edges consistently exhibit lower noise levels compared to those with straight bars, demonstrating the superior noise reduction of the serrated design.

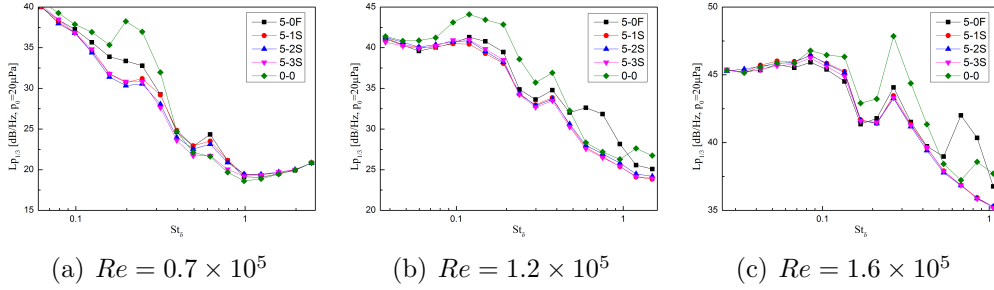


Figure 6: Sound power level for NACA 633418 airfoil with trailing edge serrations

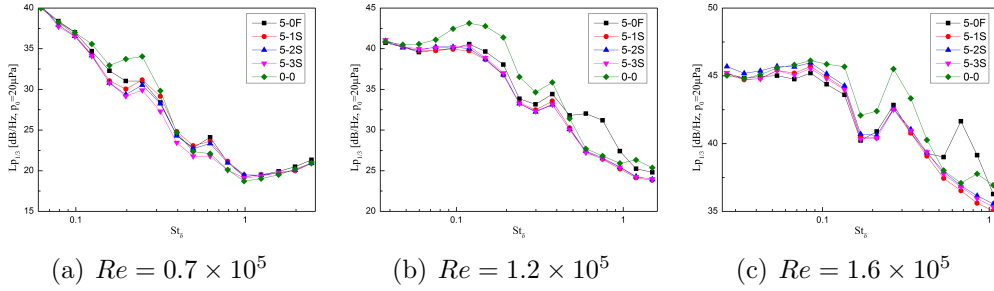


Figure 7: Sound power level for NACA 634421 airfoil with trailing edge serrations

The variation of noise reduction frequency ranges with Reynolds number ( $Re$ ) reveals the effectiveness of trailing edge serrations under different flow conditions. Using the NACA 634421 airfoil as a case study, this study examines how the noise reduction performance of serrations changes with varying Reynolds numbers, highlighting the interplay between flow characteristics and aeroacoustic phenomena. Several noteworthy observations can be concluded. Trailing edge serrations consistently demonstrate their capacity to reduce noise levels. Compared to the original airfoil, serrations are effective in reducing noise across both low-to-medium and high frequencies. When compared to an airfoil with straight trailing edges, serrations exhibit greater noise reduction mainly in the mid-to-high frequency range. The influence

of serration wavelength ( $\lambda$ ) or width-to-height ratio ( $\lambda/h$ ) on sound power level is minimal, contrary to the observation that larger wavelength serrations provided better noise reduction performance compared to smaller wavelength serrations in Moreau et al. [17, 18] and Celik et al. [20]. However, noise reduction tends to improve as the serration wavelength or width-to-height ratio decreases.

Fig. 8 shows noise reduction regions as a function of inflow wind speed and frequency, with bounds confined by two critical Strouhal numbers. The contour colors indicate the magnitude of noise reduction.

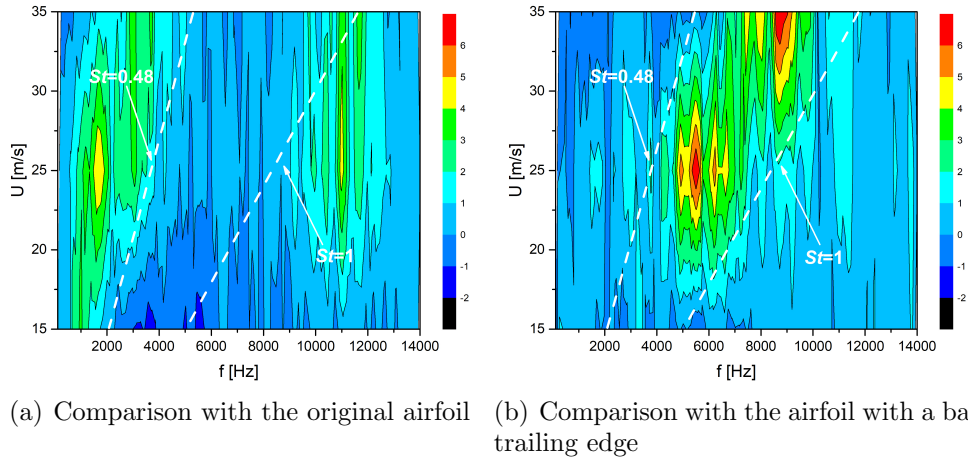


Figure 8: Distribution of noise reduction with respect to frequency ( $f$ ) and wind speed ( $U$ )

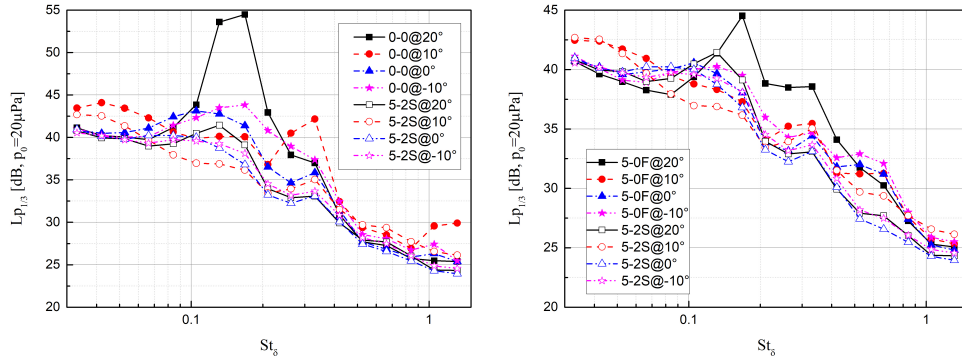
The plots in Fig. 8 (a) and (b) reveal distinct patterns of noise reduction. Serrations consistently demonstrate superior noise mitigation compared to airfoils with or without bar trailing edges, making them the preferred choice across various frequency ranges. The noise reduction zones are bounded by Strouhal numbers  $St_u = 1$  and  $St_l = 0.48$ , indicating the effective frequency ranges of the serrations. Additionally, the broader noise reduction zone at higher Reynolds numbers suggests that the effectiveness of serrations increases with Reynolds number.

### 3.2. Impact of Angle of Attack

The angle of attack significantly impacts the performance of airfoil trailing edge modifications. Changes in the angle of attack alter the flow characteristics over the airfoil, affecting noise generation mechanisms. Investigating

how trailing edge modifications interact with different angles of attack offers valuable insights into their effectiveness under various operating conditions.

Fig. 9 compares the noise levels between the NACA 634421 airfoil with and without serrated trailing edges under a Reynolds number of  $Re = 1.2 \times 10^5$ , with the 5-2S configuration selected as the experimental group. The airfoil without a trailing edge exhibits noticeable tonal noise, approximately 10 dB, within the dimensionless frequency range of  $0.2 > St > 0.1$  at a high angle of attack ( $20^\circ$ ), which is primarily due to flow separation. The serrated trailing edge effectively mitigates this tonal noise. Similarly, the airfoil with a bar trailing edge also generates prominent tonal noise around  $St \approx 0.168$  at a high angle of attack ( $20^\circ$ ), which the serrated trailing edge successfully eliminates. Across the four different angles of attack tested, the serrated trailing edge consistently demonstrates significant noise reduction within a certain frequency range, both in comparison to the airfoil without a trailing edge and the one with a bar trailing edge.



(a) Airfoil with serrated trailing edge vs. original airfoil (b) Airfoil with serrated trailing edge vs. bar trailing edge

Figure 9: Sound pressure level ( $L_P$ ) as a function of angle of attack for the NACA 634421 airfoil with and without serrated trailing edges

Fig. 10 and Fig. 11 show the effect of the angle of attack on noise reduction for the NACA 633418 and NACA 634421 airfoils, respectively. Noise reduction is calculated as the difference in sound power level between the 5-2S serrated trailing edge and the reference cases.

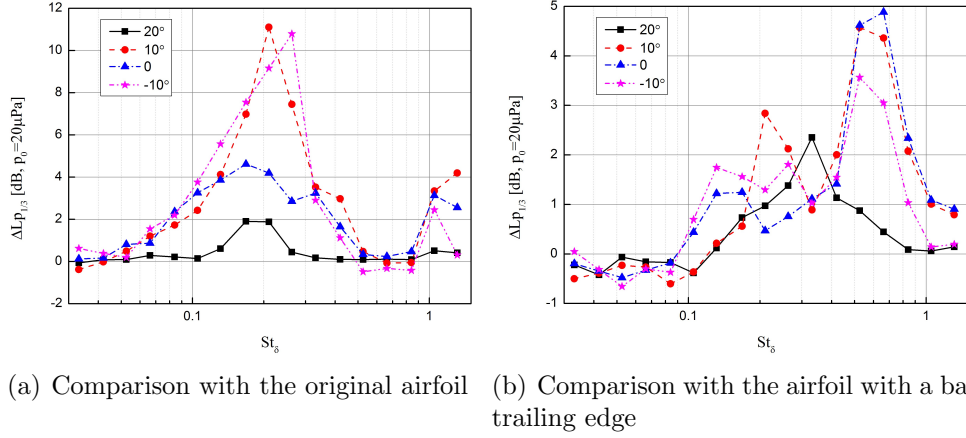


Figure 10: Noise reduction ( $\Delta L_P$ ) relative to the baselines as a function of angle of attack for the NACA 633418 airfoil with serrated trailing edges

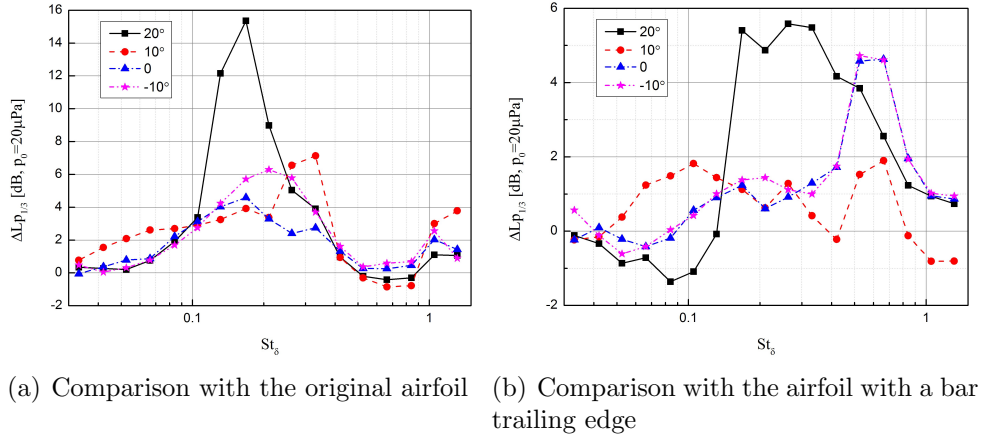


Figure 11: Noise reduction ( $\Delta L_P$ ) relative to the baseline airfoil as a function of angle of attack for the NACA 634421 airfoil with serrated trailing edges

The effectiveness of serrated trailing edges in reducing noise varies with the angle of attack for different airfoil profiles, leading to distinct noise reduction patterns in terms of frequency range and amplitude. For the NACA 633418 airfoil, the serrated trailing edge performs best at angles of  $-10^\circ$  and  $10^\circ$ , achieving noise reductions over 10 dB across a broad frequency range from  $St = 0.1$  to  $St = 1.0$ . This is likely due to the thinner profile of the

NACA 633418, which optimizes its aerodynamic performance at moderate angles of attack, effectively reducing vortex shedding and turbulence over a wide frequency range. In contrast, the NACA 634421 airfoil achieves the most significant noise reduction at an angle of  $20^\circ$ , with reductions exceeding 15 dB. The thicker profile of the NACA 634421 is optimized for higher angles of attack, significantly reducing noise by minimizing flow separation and reattachment regions.

Across different angles of attack, the bar trailing edge consistently shows inferior noise reduction performance compared to the serrated trailing edge for both airfoils tested. The maximum noise reduction difference between the serrated and bar trailing edges can reach up to 5 dB, with the serrated trailing edge being more effective across most frequency ranges.

### *3.3. Impact of Serration Height*

Fig. 12 and Fig. 13 demonstrate the influence of serration height on noise reduction for the NACA 633418 and NACA 634421 airfoils across different Reynolds numbers. While the effect of serration height on sound power level appears modest at lower Reynolds numbers, its impact becomes more pronounced at higher Reynolds numbers. The limited influence at lower Reynolds numbers may be attributed to the reduced energy in the flow, where the smaller scale of turbulent structures interacting with the serrations results in minimal noise attenuation. As the Reynolds number increases, the flow becomes more turbulent, and the interaction between the serrations and the larger turbulent eddies enhances noise reduction.

The size of the serrations plays a role in this process, though the effects were not clearly observed in our experiments. Larger serrations are expected to interact more effectively with dominant turbulent structures in the flow field, potentially disrupting coherent vortices that contribute to noise generation. This interaction could also influence aerodynamic performance by modifying the wake structure and possibly reducing drag. While longer serrations generally provide better noise reduction, consistent with Howe’s findings [31, 32] that greater serration height enhances noise reduction, it is important to recognize that Howe’s theory is based on idealized assumptions. His theory primarily links noise reduction to the rate of vorticity intersecting streamlines, but it does not fully account for the complex vortex dynamics near the airfoil trailing edge, where intricate interactions between the flow and sound fields, influenced by serration size, can affect both noise characteristics and aerodynamic performance.

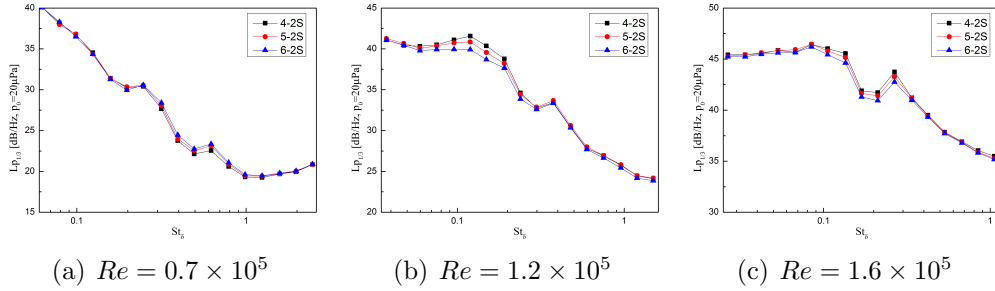


Figure 12: Sound pressure level ( $L_P$ ) as a function of serration height for the NACA 63318 airfoil with serrated trailing edges

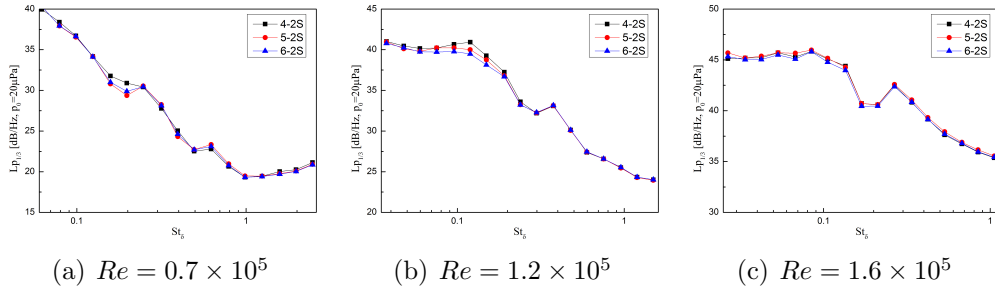


Figure 13: Sound pressure level ( $L_P$ ) as a function of serration height for the NACA 634421 airfoil with serrated trailing edges

### 3.4. Sound Field Directivity

The sound pressure levels shown in Fig. 14 represent the original intensities received by the microphones at their respective positions. Fig. 14 shows the sound directivity pattern for the NACA 633418 airfoil at a Reynolds number of  $1.2 \times 10^5$ . Several key observations about noise propagation characteristics and the effectiveness of different trailing edge modifications can be revealed. At low to medium frequencies, around 400 Hz, both straight-edge and serrated trailing edges show minimal impact on noise reduction and do not significantly alter the acoustic directivity patterns of the airfoil noise. As the frequency increases to 1000 Hz and beyond, both straight-edge and serrated trailing edges demonstrate a noticeable reduction in sound intensity. However, these modifications do not change the inherent acoustic directivity characteristics of the airfoil. For instance, at 1000 Hz, the

highest noise intensity is observed in directions approximately perpendicular to the airfoil surface, and this pattern remains unchanged with trailing edge modifications. Serrated trailing edges notably outperform straight-edge modifications in noise reduction, particularly at frequencies above 3150 Hz. The serrated configurations consistently show lower noise levels compared to straight edges, indicating their superior efficacy in mitigating noise at higher frequencies. This observation is consistent with the findings of Lyu et al. [33], which emphasized that primary noise reduction arises from interference effects near the trailing edge and highlighted substantial alterations in directivity characteristics at high frequencies. However, Tian et al. [34] demonstrated that trailing edge serrations can modify directivity characteristics.

The directivity results for the NACA 634421 airfoil exhibit similar trends and are not explicitly presented here, as the overall patterns and observations closely align with those of the analyzed configurations. Overall, the findings suggest that while trailing edge modifications can significantly reduce noise levels, especially at higher frequencies, they do not fundamentally alter the directivity characteristics of the airfoil’s acoustic emissions.

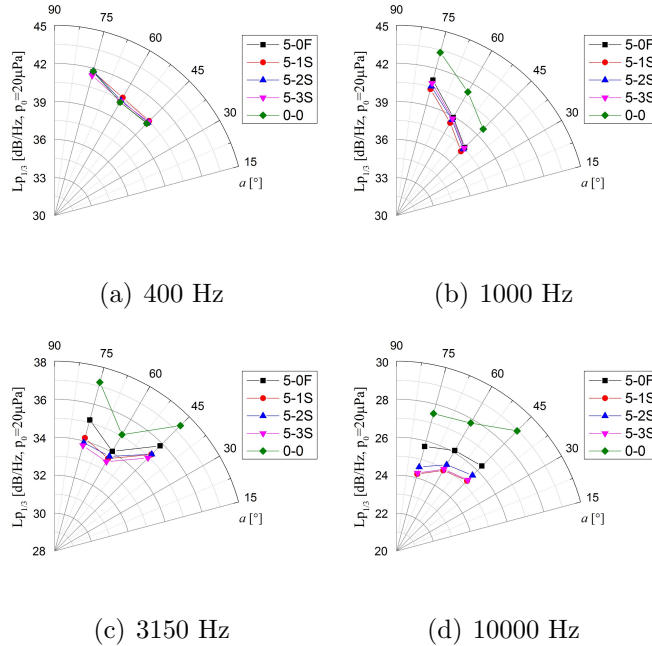


Figure 14: Sound directivity of NACA 633418 airfoil at  $Re = 1.2 \times 10^5$

## 4. Wake Flow Measurement

### 4.1. Velocity Measurement Setup

Fig. 15 shows the spatial arrangement of components within the hot wire measurement system, using Dantec Dynamics A/S products. The experiment utilized the 55P13 thermal wire probe, featuring a 90° bend, a hot wire diameter of 5  $\mu\text{m}$ , and a length of 1.25 mm. This design minimizes interference with the flow field and has a maximum response frequency of 90 kHz. The three-dimensional displacement device employs a helical micro-displacement tool, providing high-resolution measurements with a precision of up to 0.05 mm.

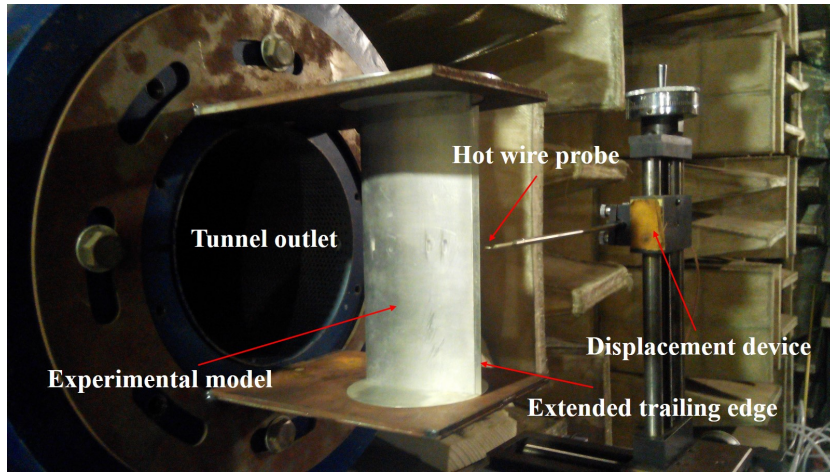


Figure 15: Hot wire measurement setup

Velocity measurements were conducted on the wake flow of three different experimental models: the original airfoil (0-0 model), the airfoil with a straight edge (5-0F model), and three airfoil models with serrated edges (5-XS, where X is 1, 2, or 3). The arrangement and numbering of measurement points are depicted in Fig. 16. For instance, measurement point "12" is located 2 mm downstream of the trailing edge in the pressure surface direction, with a 2 mm offset. Other measurement points are similarly referenced using Fig. 16.

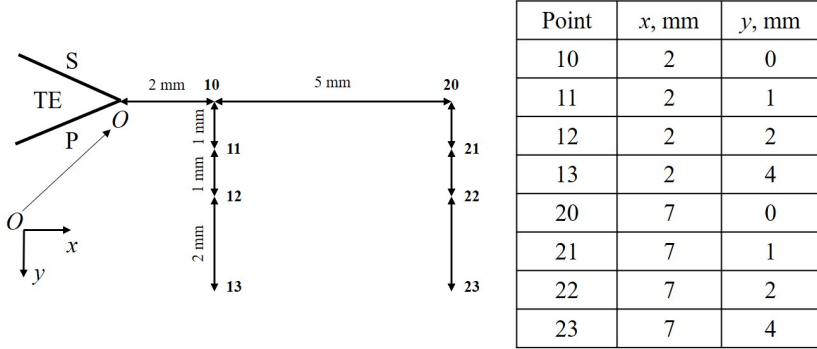


Figure 16: Measurement point locations

#### 4.2. Flow Field Measurement Results

Fig. 17 shows the mean velocity and fluctuation velocity measurements for the NACA 634421 airfoil with various trailing edge configurations at a Reynolds number of  $1.2 \times 10^5$ . The mean and fluctuation velocities at distances of 2 mm and 7 mm from the trailing edge apex are shown in Fig. 17(a) and Fig. 17(b), respectively. The horizontal axis indicates the offset distance from the trailing edge apex, as depicted in Fig. 16. The original and straight-edge airfoils exhibit the lowest mean velocities, while the serrated airfoils, particularly with the largest serration, show higher mean velocities. Fluctuation velocity generally decreases with distance from the trailing edge, and serrations effectively reduce fluctuation intensity at multiple points. These results indicate that serrated trailing edges enhance streamwise turbulence reduction.

The observed correlation between reduced wake fluctuating velocities and noise reduction may be explained by the interaction between the serrations and the trailing edge flow. Serrations likely disrupt coherent vortex structures in the wake, breaking them into smaller, less energetic eddies that generate less noise. This disruption reduces the strength of the velocity fluctuations in the wake, which is directly linked to the sound generated by the trailing edge. The reduction in fluctuating velocities near the trailing edge, therefore, leads to a decrease in noise levels.

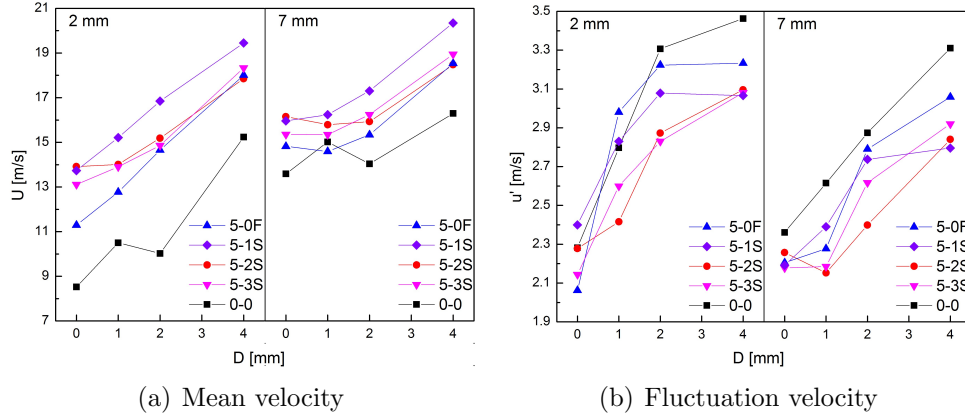


Figure 17: Velocity measurement for the NACA 634421 airfoil ( $Re = 1.2 \times 10^5$ )

Fig. 18 displays the power spectral density (PSD) of turbulent velocity fluctuations at measurement points 10 and 20 for  $Re = 1.2 \times 10^5$ . These points, located downstream of the trailing edge, are highly influenced by the flow field. The original airfoil exhibits the highest PSD in the mid-low frequency range (300~4000 Hz), with differences up to 4 dB, correlating with noise reduction ranges. This indicates that reducing streamwise fluctuations near the trailing edge contributes to noise reduction. Serrations disrupt larger vortex structures, with finer serrations proving more effective. High-frequency turbulence remains unaffected, following a  $-2.5$  power law, consistent with Ref [22].

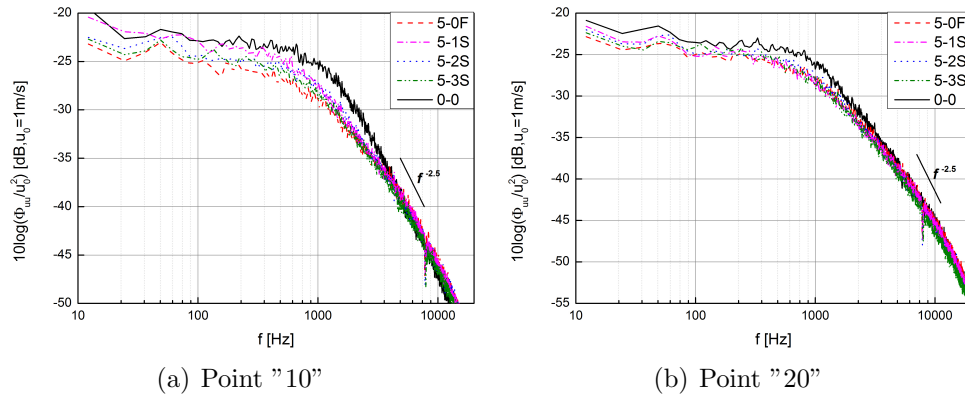


Figure 18: PSD of turbulent velocity fluctuations for NACA 634421 at  $Re = 1.2 \times 10^5$

While these results suggest a causal relationship between reduced wake fluctuations and noise reduction, the empirical data primarily indicate a correlation. Further experimentation, particularly involving direct measurements of the vortex dynamics and their contribution to noise generation, would be beneficial to validate this connection and fully understand the underlying mechanisms.

Fig. 19 shows the autocorrelation maps of turbulent velocity fluctuations for the original airfoil (0-0) and the 5-2S serrated trailing edge at 2 mm downstream, for  $Re = 1.2 \times 10^5$ . The autocorrelation map for the 0-0 model reveals a broader high-value region and a narrower mid-low-value region, indicating more persistent turbulence structures compared to the 5-2S model. This observation suggests that serrations effectively reduce the correlation of flow near the sound source, thereby diminishing the efficiency of the sound source and contributing to noise reduction.

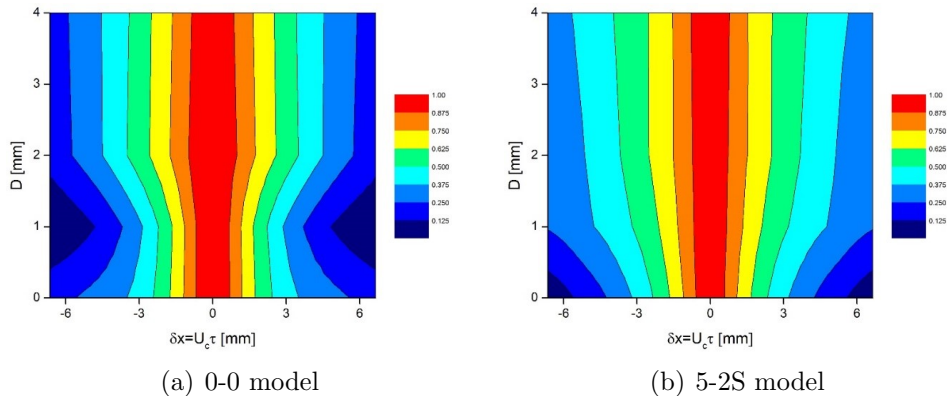


Figure 19: Autocorrelation of turbulent velocity fluctuations at 2 mm downstream of the trailing edge

The characteristic eddy scale,  $L_u(x)$ , is estimated using the autocorrelation function of the fluctuating velocity, denoted as  $R_{uu}(x, \tau)$ . The autocorrelation function at location  $x$  is defined as:

$$R_{uu}(x, \tau) = \langle u'(x, t)u'(x, t + \tau) \rangle \quad (4)$$

where  $u'(x, t)$  represents the fluctuating velocity component at time  $t$  and position  $x$ , and  $\tau$  is the time lag. We disregard the starting time, thus setting  $t = 0$ . The characteristic eddy scale is determined by finding the time lag  $\tau_0$

at which the autocorrelation function decays to half of its maximum value, as shown in Eq. (5):

$$\frac{R_{uu}(x, \tau_0)}{R_{uu}(x, 0)} = 0.5 \quad (5)$$

The eddy scale is then given by Eq. (6):

$$L_u(x) = U_c \tau_0 \quad (6)$$

where  $U_c$  is the convection velocity of the eddies, typically approximated as  $U_c = 0.7U_0$ , with  $U_0$  representing the freestream velocity. Therefore, at a given Reynolds number ( $Re$ ), the eddy scale  $L_u(x)$  depends on the position  $x$  and the corresponding time lag  $\tau_0$ .

To facilitate a comprehensive comparison of the autocorrelation functions and characteristic eddy scales across various trailing edge configurations, these metrics are presented together in a single graph, as shown in Fig. 20. The labels  $l_{c1}$  indicate the characteristic eddy scales for each type of trailing edge.

Fig. 20 illustrates that the largest turbulent length scales are associated with the 5-0F and 0-0 trailing edges. In contrast, serrated trailing edges, especially those with larger serrations, exhibit reduced turbulent length scales. This reduction in the characteristic eddy scale indicates that serrations effectively disrupt larger vortex structures, leading to a decrease in aeroacoustic noise intensity. Moreover, finer and longer serrations have a more pronounced impact on altering the vortex scale in the flow field, further enhancing their noise reduction capability. These measurements indicate that the primary reason for noise reduction by serrated trailing edges may be the alteration of the flow field near the source location, rather than changes in the radiation efficiency of the source [35, 36, 33, 37, 38, 39]. Another possible noise reduction mechanism is destructive interference of the scattered surface pressure [33], but cannot be validated in this study. There are significant observed discrepancies between numerical and experimental results, underscoring the need for further investigation and a deeper understanding of the underlying mechanisms involved in the noise reduction process.

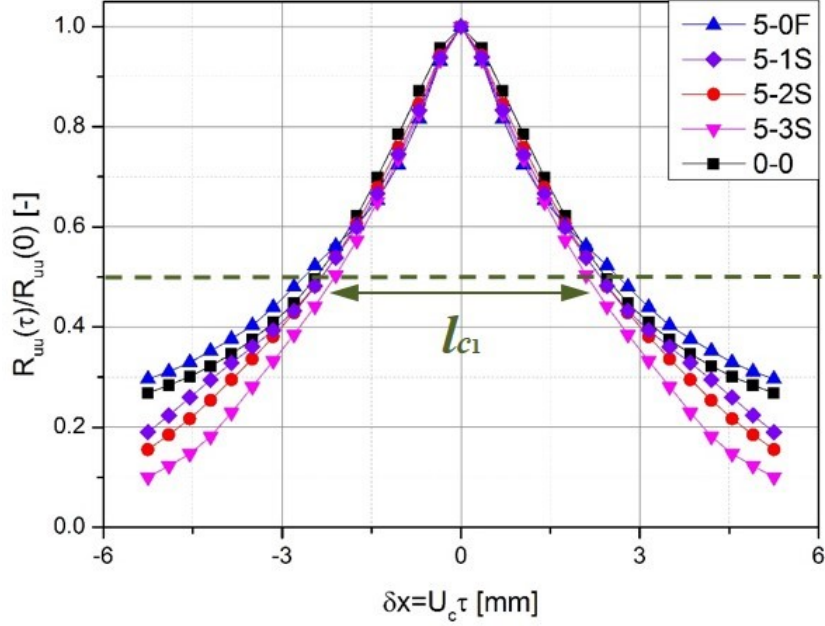


Figure 20: Autocorrelation of different trailing edges at measurement point “10” for  $Re = 1.2 \times 10^5$

## 5. Conclusions

This study offers a detailed experimental analysis of noise reduction achieved with airfoils featuring serrated trailing edges in a low turbulence wind tunnel. The research is divided into two main segments: acoustic spectral characteristics and wake flow field measurements. The first segment evaluates the influence of several factors on sound power level, including Reynolds number, angle of attack, serration parameters, and model type, along with far-field sound radiation patterns. The second segment investigates the relationship between noise reduction and flow field characteristics, focusing on fluctuating velocities at specific measurement points. This part examines how changes in the wake flow field correlate with variations in noise reduction performance.

This study provides new insights into the effects of serrated trailing edges on noise reduction, particularly across a broader frequency range than previously reported in the literature. While past research primarily associates serrated trailing edges with noise reduction at low to mid frequencies, our findings demonstrate effectiveness across both low-to-mid and high frequencies, with the most pronounced reduction occurring in the mid-to-high fre-

quency range when compared to straight trailing edge airfoils. The noise reduction range is bounded by Strouhal numbers  $St_u = 1$  and  $St_l = 0.48$ . Contrary to common assumptions, the geometry of the serrations does not play a critical role in noise reduction under the experimental conditions in this study. The serrated trailing edges show variable noise reduction effectiveness depending on the angle of attack and airfoil profile, with noise reduction observed across all four tested angles of attack within a specific frequency range. Moreover, while serration modifications substantially reduce noise, particularly at higher frequencies, they do not significantly alter the directivity pattern of the airfoil's acoustic emissions.

Wake flow velocity spectra measurements reveal a clear correlation between reduced wake turbulence and noise reduction. Serrated trailing edges effectively lower the power spectral density of turbulent velocity fluctuations and reduce the turbulent length scales near the sound source, effectively disrupting larger vortex structures and potentially decreasing the efficiency of the noise-generating mechanisms. While this relationship is promising, further experimental validation is required to strengthen these findings.

Future research should expand upon these findings by integrating simultaneous sound and flow field measurements of serrated trailing edge noise reduction in larger anechoic wind tunnels (diameter  $> 400$  mm) or real-world wind turbine settings. Employing flow visualization techniques with larger models and serrated trailing edges could provide deeper insights into the underlying mechanisms of noise reduction. Additionally, high-fidelity numerical simulations are essential for capturing accurate results, facilitating a more comprehensive understanding of the noise reduction phenomena. Incorporating analytical models may further elucidate the mechanisms involved in noise reduction.

### **Data availability**

The data that support the findings of this study are available from the corresponding author upon reasonable request.

### **References**

- [1] P. Kaewniam, M. Cao, N. F. Alkayem, D. Li, E. Manoach, Recent advances in damage detection of wind turbine blades: A state-of-the-art review, *Renewable and Sustainable Energy Reviews* 167 (2022) 112723.

- [2] B. Hoen, R. Darlow, R. Haac, J. Rand, K. Kaliski, Effects of land-based wind turbine upsizing on community sound levels and power and energy density, *Applied Energy* 338 (2023) 120856.
- [3] B. Kosasih, H. S. Hudin, Influence of inflow turbulence intensity on the performance of bare and diffuser-augmented micro wind turbine model, *Renewable Energy* 87 (2016) 154–167.
- [4] J. Sørensen, 2.08 - aerodynamic analysis of wind turbines, in: A. Sayigh (Ed.), *Comprehensive Renewable Energy*, Elsevier, Oxford, 2012, pp. 225–241.
- [5] M. F. Barone, Survey of techniques for reduction of wind turbine blade trailing edge noise. (2011).
- [6] S. Deshmukh, S. Bhattacharya, A. Jain, A. R. Paul, Wind turbine noise and its mitigation techniques: A review, *Energy Procedia* 160 (2019) 633–640.
- [7] J. Pinder, Mechanical noise from wind turbines, *Wind engineering* (1992) 158–168.
- [8] S. Oerlemans, Wind turbine noise: primary noise sources (2011).
- [9] T. F. Brooks, D. S. Pope, M. A. Marcolini, Airfoil self-noise and prediction, Technical Report, 1989.
- [10] M. Herr, W. Dobrzynski, Experimental investigations in low-noise trailing edge design., *AIAA journal* 43 (2005) 1167–1175.
- [11] M. Herr, Design criteria for low-noise trailing-edges, in: 13th AIAA/CEAS aeroacoustics conference (28th AIAA aeroacoustics conference), 2007, p. 3470.
- [12] A. Finez, M. Jacob, E. Jondeau, M. Roger, Broadband noise reduction with trailing edge brushes, in: 16th AIAA/CEAS aeroacoustics conference, 2010, p. 3980.
- [13] A. Suryadi, C. Jätz, J. Seume, M. Herr, Identifying the flap side-edge noise contribution of a wind turbine blade section with an adaptive trailing edge, *Wind Energy* 26 (2023) 64–75.

- [14] T. Geyer, E. Sarradj, C. Fritzsche, Measurement of the noise generation at the trailing edge of porous airfoils, *Experiments in fluids* 48 (2010) 291–308.
- [15] M. Zhang, T. P. Chong, Experimental investigation of the impact of porous parameters on trailing-edge noise, *Journal of Sound and Vibration* 489 (2020) 115694.
- [16] S. Oerlemans, M. Fisher, T. Maeder, K. Kögler, Reduction of wind turbine noise using optimized airfoils and trailing-edge serrations, *AIAA journal* 47 (2009) 1470–1481.
- [17] D. J. Moreau, L. A. Brooks, C. J. Doolan, Flat plate self-noise reduction at low-to-moderate reynolds number with trailing edge serrations, in: *Proceedings of ACOUSTICS*, 2011, pp. 2–4.
- [18] D. J. Moreau, C. J. Doolan, Noise-reduction mechanism of a flat-plate serrated trailing edge, *AIAA journal* 51 (2013) 2513–2522.
- [19] F. Avallone, W. Van Der Velden, D. Ragni, D. Casalino, Noise reduction mechanisms of sawtooth and combed-sawtooth trailing-edge serrations, *Journal of Fluid Mechanics* 848 (2018) 560–591.
- [20] A. Celik, Y. Mayer, M. Azarpeyvand, On the aeroacoustic characterization of a robust trailing-edge serration, *Physics of Fluids* 33 (2021).
- [21] L. T. L. Pereira, D. Ragni, F. Avallone, F. Scarano, Aeroacoustics of sawtooth trailing-edge serrations under aerodynamic loading, *Journal of Sound and Vibration* 537 (2022) 117202.
- [22] M. Gruber, P. Joseph, T. P. Chong, Experimental investigation of airfoil self noise and turbulent wake reduction by the use of trailing edge serrations, in: *16th AIAA/CEAS aeroacoustics conference*, 2010, p. 3803.
- [23] M. Gruber, P. Joseph, T. Chong, On the mechanisms of serrated airfoil trailing edge noise reduction, in: *17th AIAA/CEAS aeroacoustics conference (32nd AIAA aeroacoustics conference)*, 2011, p. 2781.
- [24] P. Zhou, Q. Liu, S. Zhong, Y. Fang, X. Zhang, A study of the effect of serration shape and flexibility on trailing edge noise, *Physics of Fluids* 32 (2020).

- [25] T. Dassen, R. Parchen, J. Bruggeman, F. Hagg, Results of a wind tunnel study on the reduction of airfoil self-noise by the application of serrated blade trailing edges (1996).
- [26] A. Finez, M. Jacob, M. Roger, E. Jondeau, Broadband noise reduction of linear cascades with trailing edge serrations, in: 17th AIAA/CEAS Aeroacoustics Conference (32nd AIAA Aeroacoustics Conference), 2011, p. 2874.
- [27] S. K. Singh, S. Narayanan, Control of airfoil broadband noise through non-uniform sinusoidal trailing-edge serrations, *Physics of Fluids* 35 (2023).
- [28] T. P. Chong, P. F. Joseph, An experimental study of airfoil instability tonal noise with trailing edge serrations, *Journal of Sound and Vibration* 332 (2013) 6335–6358.
- [29] T. Chong, P. Joseph, M. Gruber, Airfoil self noise reduction by non-flat plate type trailing edge serrations, *Applied Acoustics* 74 (2013) 607–613.
- [30] T. P. Chong, P. Joseph, A. Vathylakis, M. Gruber, On the noise and wake flow of an airfoil with broken and serrated trailing edges, in: 17th AIAA/CEAS aeroacoustics conference (32nd AIAA aeroacoustics conference), 2011, p. 2860.
- [31] M. S. Howe, Aerodynamic noise of a serrated trailing edge, *Journal of Fluids and Structures* 5 (1991) 33–45.
- [32] M. S. Howe, Noise produced by a sawtooth trailing edge, *The Journal of the Acoustical society of America* 90 (1991) 482–487.
- [33] B. Lyu, M. Azarpeyvand, S. Sinayoko, Prediction of noise from serrated trailing edges, *Journal of Fluid Mechanics* 793 (2016) 556–588.
- [34] H. Tian, B. Lyu, Prediction of broadband noise from rotating blade elements with serrated trailing edges, *Physics of Fluids* 34 (2022).
- [35] L. Jones, R. Sandberg, Numerical investigation of airfoil self-noise reduction by addition of trailing-edge serrations, in: 16th AIAA/CEAS aeroacoustics conference, 2010, p. 3703.

- [36] R. Sandberg, L. Jones, Reprint of: direct numerical simulations of airfoil self-noise, *Procedia IUTAM* 1 (2010) 274–282.
- [37] Y. D. Mayer, B. Lyu, H. K. Jawahar, M. Azarpeyvand, A semi-analytical noise prediction model for airfoils with serrated trailing edges, *Renewable Energy* 143 (2019) 679–691.
- [38] L. J. Ayton, Analytic solution for aerodynamic noise generated by plates with spanwise-varying trailing edges, *Journal of Fluid Mechanics* 849 (2018) 448–466.
- [39] M. B. Gelot, J. W. Kim, Effect of serrated trailing edges on aerofoil tonal noise, *Journal of Fluid Mechanics* 904 (2020) A30.